Article

Choroid plexus-mediated CSF secretion remains stable in aging rats via high and age-resistant metabolic activity

Sara D. Lolansen [1,2,10], Eszter O. Révész[1,10], Søren N. Andreassen[1,10], Marleen Trapp[3], Chiara Salio [4], Marco Sassoé-Pognetto [5], Jens Velde Andersen [6], Emil W. Westi [6], Trine L. Toft-Bertelsen [1], Jonathan H. Wardman[1], Anne-Kristine Meinild Lundby[7], Flemming Dela [7,8], Annarita Patrizi [3,9], Blanca I. Aldana [6] & Nanna MacAulay [1] ✉

Our brain is bathed in cerebrospinal fluid (CSF) that is produced by the choroid plexus. CSF serves as a dispersion route for hormones and nutrients, and a conduit for waste clearance. Age-dependent reduction in the CSF secretion rate could influence cerebral waste clearance and thereby promote cognitive deficits in the elderly. Here, we resolve age-dependent modulation of CSF dynamics and choroid plexus function by complementary in vivo determinations of intracranial pressure (ICP) and CSF secretion/absorption rates, combined with transcriptomic, morphological, and metabolic analysis of choroid plexus in aging male rats. ICP and CSF secretion rate and absorption capacity remain stable with age, and the choroid plexus retains its morphology, structural integrity, gene expression, and high metabolic rate across the tested ages. This work supports the significance of choroid plexus function for brain aging and promotes this tissue as a future target for neurodegenerative diseases associated with impaired waste clearance and cognitive decline.

Cerebrospinal fluid (CSF) continuously circulates in the mammalian brain and the cranial and spinal subarachnoid spaces[1]. Throughout life, maintenance of CSF homeostasis is vital for normal health. The CSF provides brain buoyancy and protects against mechanical insults, enables delivery of nutrients, hormones, and growth factors critical for normal brain development, and serves as a conduit for removal of metabolic waste products back into the systemic circulation[2,3]. Dysregulated CSF homeostasis is increasingly recognized as a potential contributor to various brain pathologies ranging from distorted corticogenesis in the developing brain[4], neurodegeneration in the elderly

brain[5–8], and hydrocephalic conditions, which may manifest at all ages[9,10]. An important impediment to the advancement of novel treatment strategies targeting dysregulated CSF dynamics is our currently limited understanding of how CSF dynamics change throughout the course of life.

The adult human brain produces roughly 500 mL of CSF each day[11], the majority of which arises from the secretory actions of the choroid plexus residing within the four fluid-filled ventricles of the brain[1]. The molecular mechanisms by which the choroid plexus secretes CSF and the effects of healthy ageing on the CSF secretion

[1]Department of Neuroscience, University of Copenhagen, Copenhagen, Denmark. [2]Department of Neurosurgery, University Hospital of Copenhagen - Rigshospitalet, Copenhagen, Denmark. [3]Schaller Research Group, German Cancer Research Center (DKFZ), Heidelberg, Germany. [4]Department of Veterinary Sciences, University of Turin, Grugliasco, Italy. [5]Department of Neurosciences Rita Levi Montalcini, University of Turin, Turin, Italy. [6]Department of Drug Design and Pharmacology, University of Copenhagen, Copenhagen, Denmark. [7]Xlab, Department of Biomedical Sciences, University of Copenhagen, Copenhagen, Denmark. [8]Laboratory of Sports and Nutrition Research, Riga Stradins University, Riga, Latvia. [9]Interdisciplinary Center for Neuroscience, Heidelberg University, Heidelberg, Germany. [10]These authors contributed equally: Sara D. Lolansen, Eszter O. Révész, Søren N. Andreassen. ✉e-mail: macaulay@sund.ku.dk

apparatus and the associated CSF dynamics remain incompletely understood. The choroid plexus of humans and mice displays age-dependent morphological changes such as flattening of the epithelium, thickening of the basement membrane, and a reduction in the number and the length of the microvilli facing the CSF-filled ventricles[12–14]. These structural changes have been speculated to be accompanied by a reduced functional capacity, evidenced by mitochondrial alterations[12] and decreased enzymatic activity[15]. These morphological changes may either not affect CSF secretion rates[16,17] or may increase[18–20] or reduce[21–25] CSF secretion with age. An age-dependent reduction in CSF secretion, together with a concomitant decline in fluid exchange between the CSF and the brain parenchyma[6] could potentially hinder clearance of metabolic waste products and lead to accumulation of toxic substances, ultimately promoting neurodegeneration and cognitive decline in the elderly population[5–7,26,27]. Here, we show that healthy ageing rats sustain their CSF secretion and absorption rates, and thus intracranial pressure (ICP), with intact choroid plexus morphology, transcriptomics, metabolic rate, and mitochondrial function.

Results

Brain water content declines with maturity but remains stable in aging

To elucidate age-dependent changes in brain fluid dynamics, we employed male rats of the six different age groups: 1, 3, 6, 12, 18, and 24 months of age (Fig. 1a). An increase in body weight was observed at the first two time points, after which the weight plateaued (1 M: 136 ± 2 g; 3 M: 419 ± 7 g; 6 M: 525 ± 14 g; 12 M: 541 ± 26 g; 18 M: 558 ± 22 g; 24 M: 492 ± 34 g, $n = 6$ in each group, Fig. 1b). A similar age-dependent increase in brain weight was observed in the young age groups (1 M: 1.67 ± 0.02 g; 3 M: 1.92 ± 0.07 g; 6 M: 2.15 ± 0.05 g; 12 M: 2.19 ± 0.06 g, 18 M: 2.13 ± 0.08 g; 24 M: 2.19 ± 0.07 g, $n = 6$ in each group, Fig. 1c) with the youngest group of rats (1 M) displaying a significantly higher relative brain weight (>1%) compared to the remaining age groups (<0.5%), $P < 0.001$, Fig. 1d. To determine the brain water content, we employed the wet-dry technique[28], which revealed a significantly higher brain water content in the younger rats (1 M: $79.8 \pm 0.1\%$, $n = 6$) compared to all other age groups (3 M: $78.0 \pm 0.1\%$; 6 M: $77.2 \pm 0.3\%$; 12 M: $76.5 \pm 0.1\%$; 18 M: $76.5 \pm 0.2\%$; 24 M: $76.3 \pm 0.2\%$, $n = 6$ in each group, $P < 0.001$), with the brain water content plateauing at the 6–12 M age and remaining stable in aging (Fig. 1e).

ICP remains stable with age

To reveal whether the age-dependent brain water content translated to changes in ICP, we measured the ICP in each age group with an epidural pressure probe placed in anaesthetized, mechanically ventilated rats (Fig. 1f). The 1-month old rats displayed a tendency towards a lower ICP (1 M: 2.50 ± 0.39 mmHg, $n = 6$) but with no significant differences across the age groups (3 M: 3.95 ± 0.30 mmHg; 6 M: 3.85 ± 0.38 mmHg; 12 M: 3.22 ± 0.39 mmHg; 18 M: 3.93 ± 0.66 mmHg, 24 M: 4.28 ± 0.59 mmHg, $n = 6-7$, Fig. 1g). The results suggest that the ICP remains stable with aging.

CSF drainage capacity remains stable with age

To resolve if the stable ICP aligned with undisturbed CSF dynamics, we determined the CSF drainage capacity as the resistance to CSF outflow (R_{out}) in the six age groups. The ICP was continuously monitored in anaesthetized and ventilated rats during lateral ventricular infusion of pre-heated aCSF in rates of 5, 10, and 15 μl/min (Fig. 1h). The ICP at the end of each infusion step was employed to calculate the R_{out} (see Methods). There was no significant difference in CSF drainage capacity across the six age groups ((in mmHg/min/μl) 1 M: 0.58 ± 0.09; 3 M: 0.60 ± 0.06; 6 M: 0.74 ± 0.09; 12 M: 0.63 ± 0.06; 18 M: 0.66 ± 0.08; 24 M: 0.63 ± 0.13, $n = 6-7$, Fig. 1i). Therefore, the findings suggest that the CSF drainage capacity remains intact with healthy aging.

CSF secretion remains stable with age

To quantify the contribution of CSF secretion to the age-resistant ICP, the CSF secretion rate was determined in the six different groups of rats using the ventriculo-cisternal perfusion technique[29,30]. Here, the ventricular system of anesthetized and mechanically ventilated rats was continuously perfused with heated, equi-osmolar, and gas-equilibrated aCSF containing a fluorescent dye of high molecular weight (dextran, MW: 155 kDa) with simultaneous sampling of the perfused solution through a cisterna magna puncture. As the high molecular weight of the dextran hinders detectable dye dispersion into the surrounding brain tissue (Ref. 31 and Supplementary Fig. S5d), the CSF secretion rate can be directly obtained from the degree of dye dilution that occurs upon mixing of the perfused solution with the nascent CSF (Fig. 1j). The CSF secretion rate was significantly lower in the youngest group of rats (1 M: 4.37 ± 0.15 μl/min, $n = 6$) compared to the remaining age groups ($P < 0.05$ to $P < 0.001$), which displayed similar CSF secretion rates, except for a small, yet significant ($P < 0.05$), decrease in CSF secretion rate from 18 to 24 months of age ((in μl/min) 3 M: 6.41 ± 0.20; 6 M: 6.90 ± 0.60; 12 M: 6.79 ± 0.22; 18 M: 7.51 ± 0.43; 24 M: 5.94 ± 0.28, $n = 6-7$, Fig. 1k). Hence, the CSF secretion rate appears to remain stable with aging, although with a tendency towards a beginning reduction in the oldest age group.

No morphological remodeling in aging choroid plexus

With minimal age-dependent changes in CSF secretion rates, we determined the morphological structure of choroid plexus epithelial cells obtained from aging rats. Overall, the choroid plexus epithelial cells retained their gross ultrastructural morphology across all age groups (Fig. 2a), with no significant alterations in neither cross-sectional cell area ((in μm^2) 1 M: 365 ± 27; 3 M: 408 ± 20; 6 M: 414 ± 16; 12 M: 359 ± 8; 18 M: 414 ± 15; 24 M: 363 ± 6, $n = 3$, Fig. 2b) nor cell axis ratio (1 M: 1.07 ± 0.13; 3 M: 1.08 ± 0.01; 6 M: 0.94 ± 0.06; 12 M: 1.16 ± 0.12; 18 M: 0.90 ± 0.03; 24 M: 0.93 ± 0.06, $n = 3$, Fig. 2c). Similarly, we observed no significant age-dependent changes in microvilli length ((in μm) 1 M: 1.57 ± 0.11; 3 M: 1.37 ± 0.01; 6 M: 1.52 ± 0.14; 12 M: 1.58 ± 0.05; 18 M: 1.48 ± 0.08; 24 M: 1.54 ± 0.09, $n = 3$, Fig. 2d) or their morphology (Fig. 2e). Finally, tight junctions also appeared intact and unchanged amongst the different age groups (Fig. 2f).

Transcriptomic analysis of choroid plexus as a function of age

To reveal if age-dependent changes in CSF dynamics originated in choroid plexus function rather than morphology, we determined the transcriptomic profile of choroid plexus obtained from rats of the six different age groups by RNAseq. The overall density of gene expression was similar between the age groups (Fig. 3a), although with slight age-dependent fluctuations in genes at the lower end of the expression level (Fig. 3a insert). To elucidate the overall distribution in expression profiles amongst the different age groups, we performed a PCA plot of the different age groups. The age groups arranged into three distinct clusters containing the very young (1 month old), the young adult to adult (3, 6, and 12 months old) and the elderly rats (18 and 24 months old), Fig. 3b. We discovered that the different age groups shared expression of the vast majority (92-95%, depending on their gene library size) of genes (Fig. 3c) with 1072 genes differentially expressed over the different age groups (Supplementary Data 1, sheet S1). A number of genes was exclusively expressed within each group with the 1-month-old rats expressing the largest number of exclusive genes (288, ~2.1% of all expressed genes), followed by the 18-months old (89 genes, ~0.6%), 24-months old (72 genes, ~0.5%), and to a lesser degree the remaining age groups with ~0.2–0.3% exclusive genes (37, 31, and 19 genes for age groups 3, 6, and 12 months, respectively), Fig. 3c.

To reveal the functional characteristics of the differentially expressed genes, those recognized by the PANTHER database were assigned to a molecular function (Supplementary Data 1, sheet S2), as displayed in the enrichment plot in Fig. 3d. The highest abundance of differentially expressed genes were categorized as 'binding'
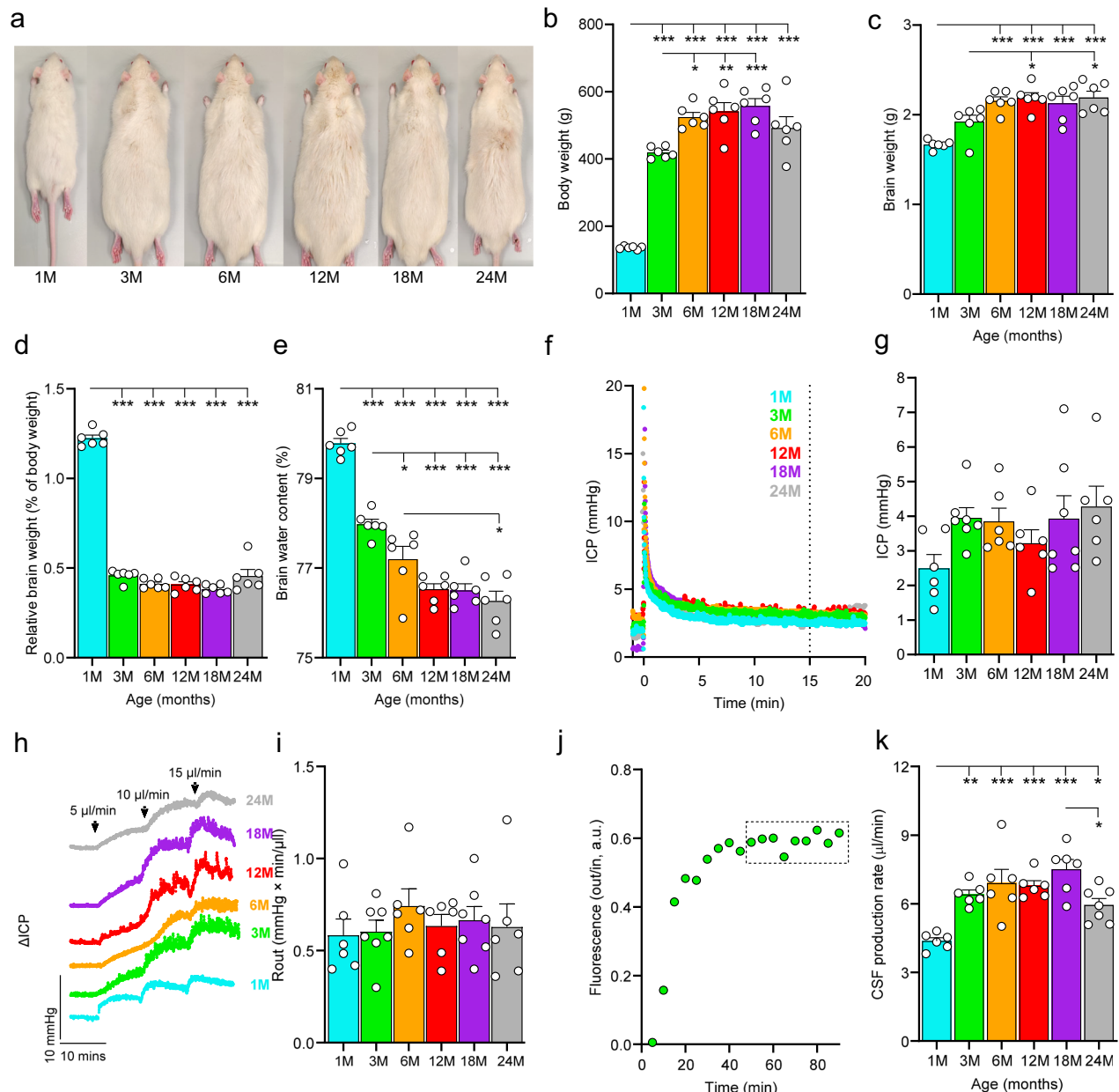
Fig. 1 | Weight and CSF dynamics as a function of age. a Representative images of the six different age groups employed in the study (1, 3, 6, 12, 18, and 24-months (M) old male Wistar rats anesthetized with ketamine/xylazin, $n = 6$ rats in each age group). **b.** Body weight of the six different age groups. **c** Brain weight of the six different age groups. **d** Relative brain weight of the six different age groups calculated as percentage of body weight. **e** Brain water content of the six different age groups calculated using the wet-dry technique (note; y-axis does not initiate at 0). **f** Representative ICP traces obtained in one rat of each age group with the peak indicating injection of 5 μl aCSF to obtain a continuous fluid column. The dashed line indicates the starting point of the last 5 min used to obtain the average ICP in each animal. **g** Averaged ICP in rats of different ages ($n = 6$ (1 M, 6 M, 12 M, 24 M) or 7 (3 M, 18 M) rats in each age group). **h** Representative ICP traces obtained in one rat of each age group undergoing resistance to CSF outflow (R_{out}) measurements.

Arrows indicate initiation of each infusion rate. **i** Resistance to CSF outflow (R_{out}) in rats of different ages ($n = 6$ (1 M, 6 M, 12 M, 24 M) or 7 (3 M, 18 M) rats in each age group). **j** Representative time course trace of the fluorescence ratio of dextran (outflow/inflow) during ventriculo-cisternal perfusion of one rat (3 M). The squared insert indicates the region used for the quantification of CSF secretion rates. **k** CSF secretion rates across the six different age groups were quantified from the fluorescence ratio of dextran ($n = 6$ (1 M, 3 M, 6 M, 12 M, 18 M) or 7 (24 M) rats in each age group. 1 M; turquoise, 3 M; green, 6 M; orange, 12 M; red, 18 M; purple, 24 M; grey. Data are presented as mean ± SEM and statistical significance was tested with one-way ANOVA followed by Tukey's multiple comparisons test. Asterisks denote statistical significance (*$P < 0.05$, **$P < 0.01$, ***$P < 0.001$). Non-significance is not illustrated for clarity. Source data are provided as a Source Data file and exact P-values in Supplementary Data 2.

(296 genes, 22%), followed by 'catalytic activity' (211 genes, 16%), 'transporter activity' (62 genes, 5%), 'molecular function regulator' (54 genes, 4%), 'molecular transducer activity' (48 genes, 4%), 'transcription regulator activity' (46 genes, 3%), 'structural molecule activity' (22 genes, 2%), and 'ATP-dependent activity' (14 genes, 1%) with the rest of the molecular functions having ≤1% genes assigned or could not be assigned a molecular function (570 genes, 43%). Quantification of the

gene expression within each category as a function of age revealed no obvious decline with aging, although with an elevated transcriptional level in all categories besides 'ATP-dependent activity' in the 1-month age group (Fig. 3e). To further elucidate the age-dependent gene expression within the choroid plexus, the differentially expressed genes were organized into protein classes, as illustrated in the enrichment plot in Fig.4a (Supplementary Data 1, sheet S2). 346 genes
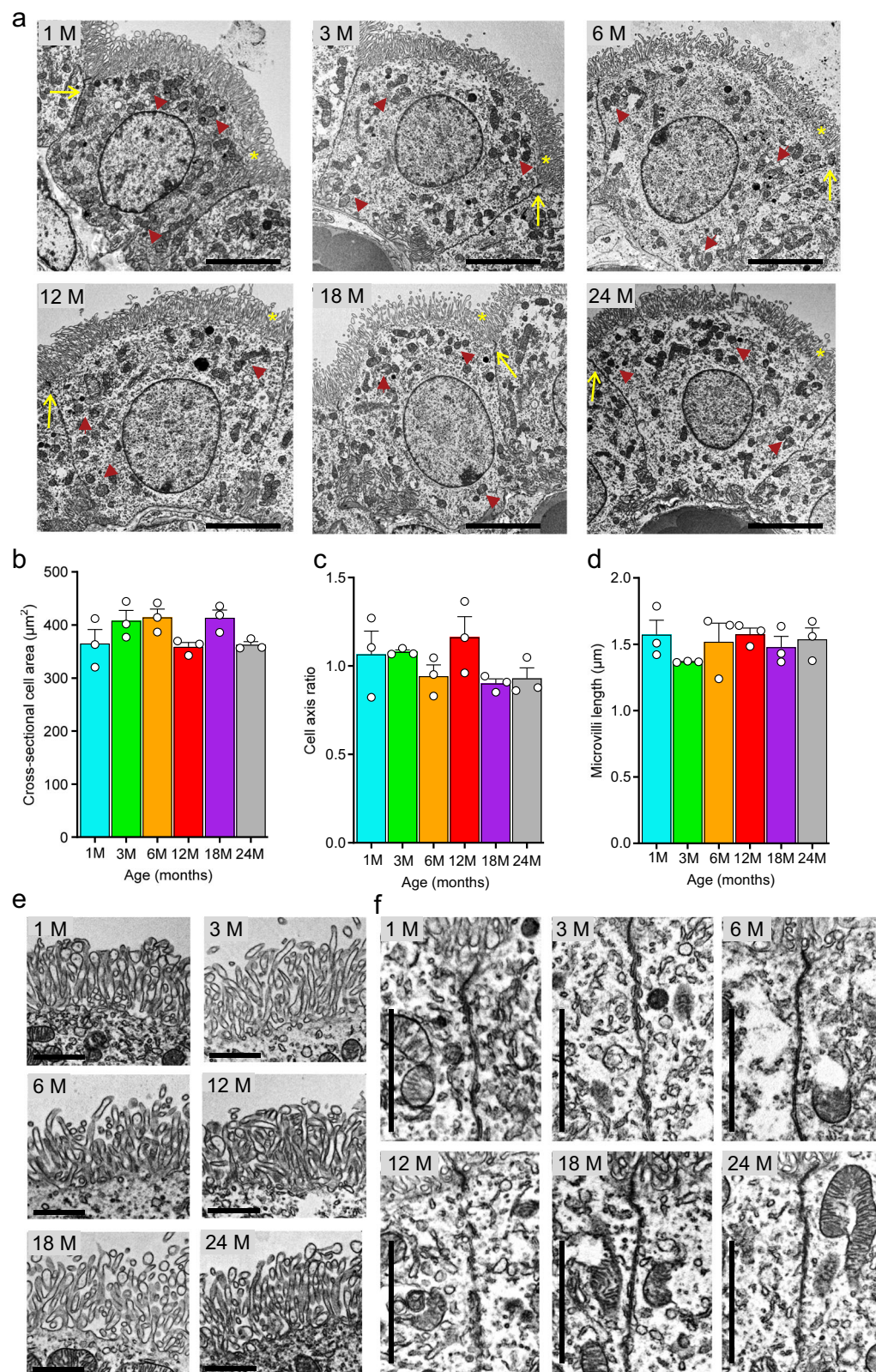
Fig. 2 | Choroid plexus epithelial cell morphology as a function of age.
a Representative TEM images of choroid plexus epithelial cells at different ages.
Asterisks indicate microvilli; arrow: tight junction; arrowhead: mitochondria.
Quantification of cross-sectional cell area (**b**), cell axis ratio (**c**), and microvilli
length (**d**). Representative high magnification TEM images of microvilli (**e**) and tight
junctions (**f**) from all age groups, $n = 3$ (each dot represents the average of seven
images per animal). 1 M; turquoise, 3 M; green, 6 M; orange, 12 M; red, 18 M; purple,
24 M; grey. Data are presented as mean ± SEM, and statistical significance was
tested with the Kruskal-Wallis test followed by Dunn's multiple comparisons test.
Non-significance is not illustrated for clarity. Scale bar 5 μm (**a**), 1 μm (**e**), 2 μm (**f**).
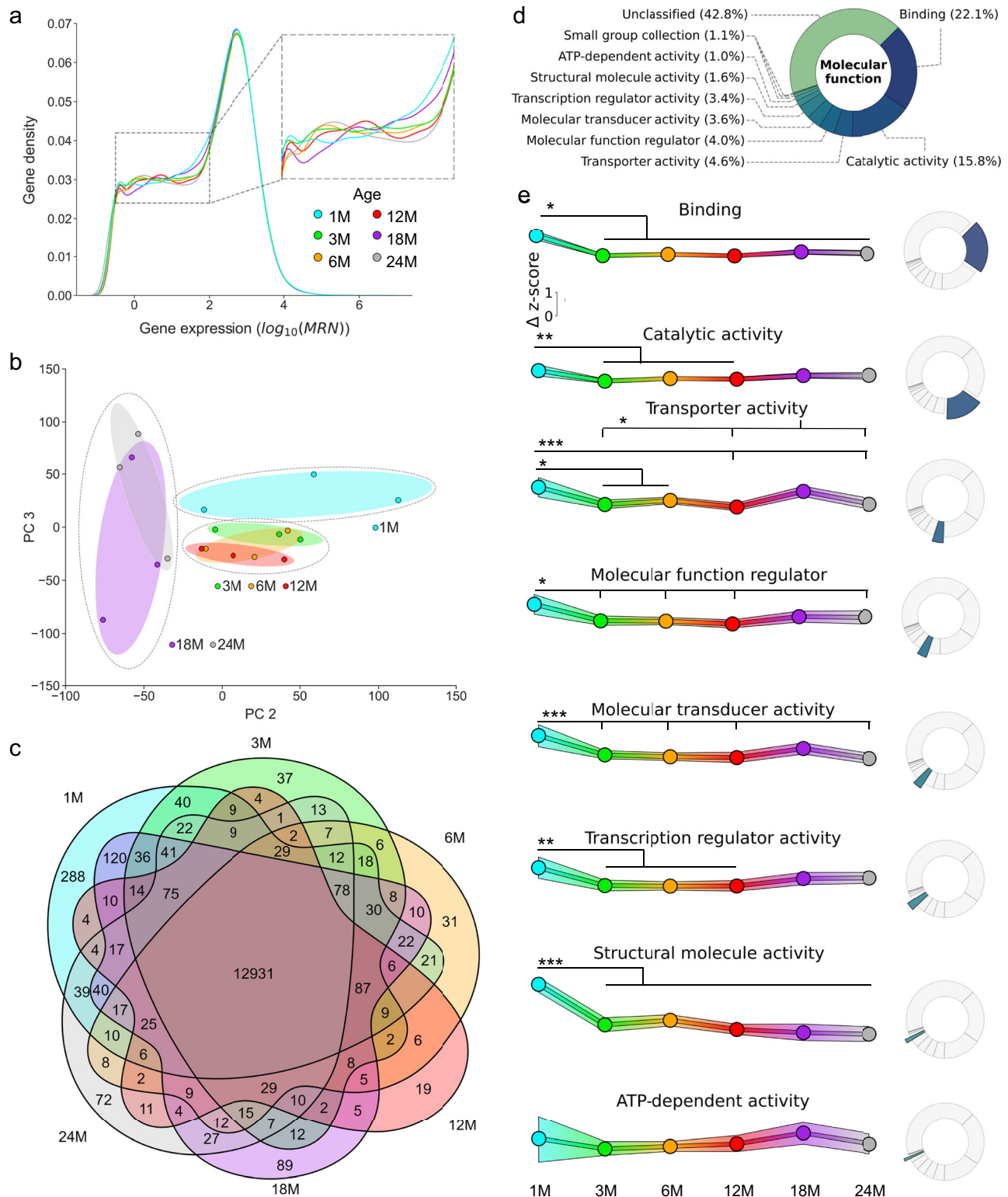Source data are provided as a Source Data file.

Fig. 3 | Differential choroid plexus gene expression as a function of age. a Gene expression density between the different age states. Gene density (y-axis) versus gene expression in $\log_{10}$(Median Ratio Normalization (MRN)) (x-axis). Insert highlights gene expression between $\log_{10}$ (MRN) of −0.5 and 2. **b** PCA plot of the different age groups with the three major clusters of age groups encircled. **c** Genes shared between the age groups (excluding genes expressed lower than 10 TMM). **d** GO enrichment analysis of the molecular functions of the differentially expressed genes. **e** Expression level of the differentially expressed genes within each category of molecular functions across all age groups. The expression levels are the z-score of the mean (circles) with the 95% confidence interval indicated as shaded area. $n = 3$. 1 M; turquoise, 3 M; green, 6 M; orange, 12 M; red, 18 M; purple, 24 M; grey. Statistical significance was tested with one-way ANOVA followed by Tukey's multiple comparisons post hoc test. Asterisks denote statistical significance between the age groups (*; $P < 0.05$, **; $P < 0.01$, ***; $P < 0.001$). Non-significance is not illustrated for clarity. Source data are provided as a Source Data file and exact P-values in Supplementary Data 2.
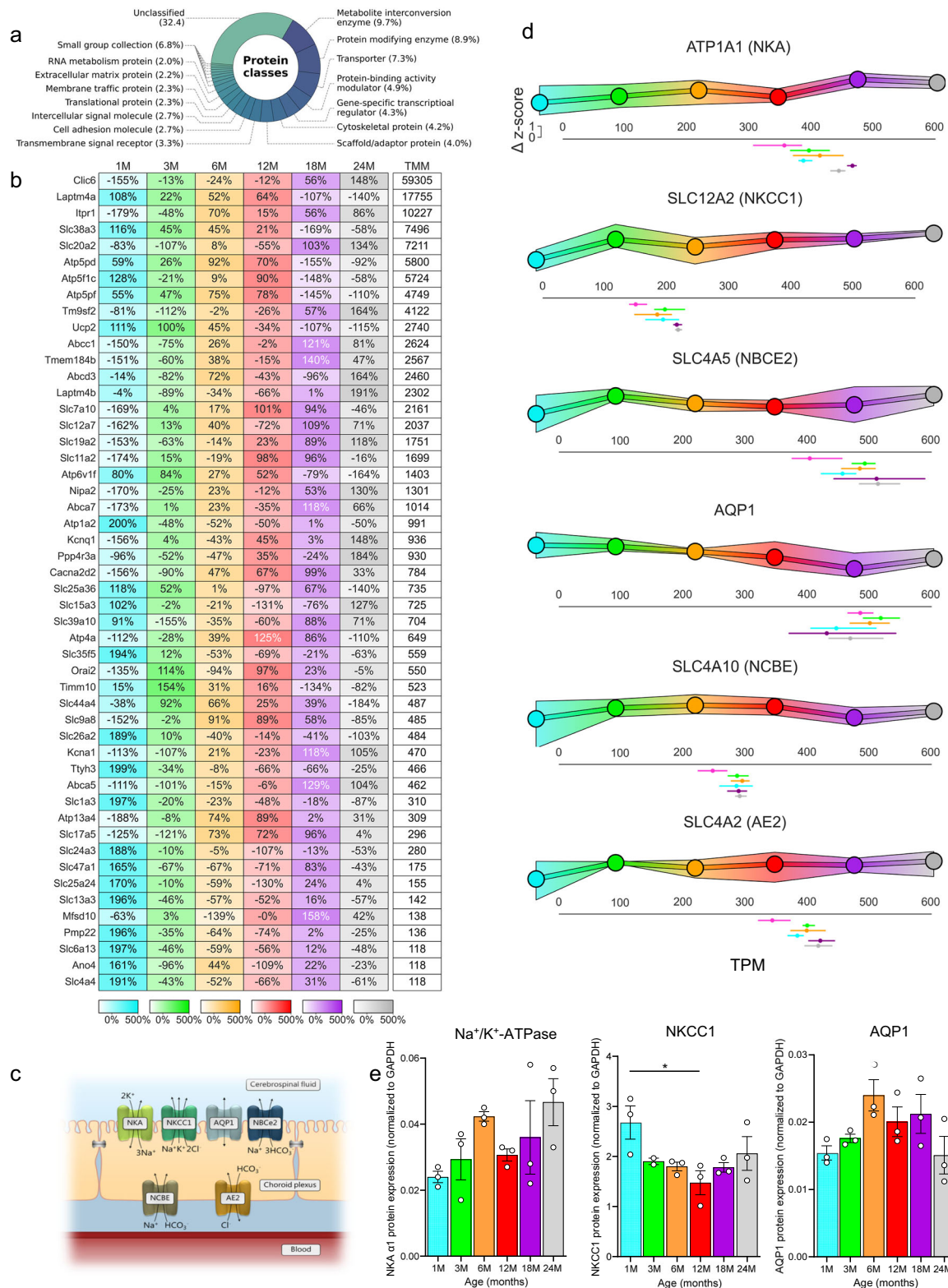
Fig. 4 | Differential expression of choroid plexus transport proteins as a function of age. a GO enrichment analysis of the differentially expressed genes in choroid plexus obtained from the different age groups into protein classes. **b** All differentially expressed proteins within the 'transporter' category with a mean of trimmed mean of M values (TMM) above 100. Listed are the gene names together with their percentage fluctuations from the mean in the 1-, 3-, 6-, 12-, 18-, and 24-months-old groups, with the average expression in TMM. **c** Schematic of choroid plexus illustrating the polarized expression of transporters implicated in CSF secretion. NCBE and NBCe2; Na+-coupled HCO3- transporters, AE2; Cl-/HCO3- exchanger, AQP1; aquaporin 1, NKCC1; Na+,K+,2Cl- cotransporter 1, NKA; Na+/K+-ATPase. Tight

junctions are marked with black bars. **d** Expression levels as a function of age illustrated as z-score of the mean (circles) with the 95% confidence interval indicated as a shaded area. The expression level of each transporter at each age is indicated in transcripts per million (TPM) below each graph, $n = 3$. **e** Quantification of Western blots (from Supplementary Fig. 2b–d) of Na+/K+-ATPase (NKA), NKCC1, and AQP1, $n = 3$, data are presented as mean ± SEM and statistical significance was tested with one-way ANOVA followed by Tukey's multiple comparisons test. Asterisks denote statistical significance (*$P < 0.05$), non-significance is not illustrated for clarity. 1 M; turquoise, 3 M; green, 6 M; orange, 12 M; red, 18 M; purple, 24 M; grey. Source data are provided as a Source Data file and exact P-values in Supplementary Data 2.

(32%) could not be assigned to a protein class, but the majority of the differentially expressed genes were assigned to the category of 'metabolite interconversion enzymes' (104 genes, 10%), followed by 'protein modifying enzymes' (96 genes, 9%), and 'transporters' (79 genes, 7%). The latter category could directly influence the CSF secretion rate and transcellular transport of metabolites etc., and their individual age-dependent expression fluctuation therefore illustrated in Fig. 4b. The table of transporters only includes genes with an expression level of 100 TMM or above, but all differentially expressed genes classified as 'Transporter' are included in Supplementary Data 1, sheet S2 – Protein class. To elucidate whether the choroid plexus capacity to clear brain waste products and toxins may reduce with age, we extracted the set of choroid plexus transcripts encoding transport families involved in these processes, i.e., the ABC transporter family and the SLC families involved in efflux of waste products[32]. The ABC transporter family increased in expression in the two eldest age groups, which contrasts the age-dependent downward trend of the other three transporter categories, and the abrupt decline in the 24 months age group for the nucleoside and peptide transporters group (Supplementary Fig. S1a). For the expression of genes encoding drug-metabolizing enzymes, one group (glutathione S-transferases and glutathione-synthesis related genes) displayed a stable expression across the age groups, whereas the three other groups ('Cytochrome P450s and epoxide hydrolases', 'flavin-containing monooxygenases', and 'UDP-glucuronosyltransferases and sulfotransferases') exhibited slight, but not statistically significant, fluctuations across the age groups (Supplementary Fig. S1b). Of the antioxidant enzymes, the group encoding heme oxygenases and biliverdin reductase displayed a tendency towards reduced expression in the older age groups (Supplementary Fig. S1c). We observed no overall age-dependent decline of transcripts encoding junctional proteins (Supplementary Fig. S1d), nor in individual transcript abundance of the expressed tight junctional proteins (claudin 1, 2, 3, 5, 9, 10, 12, 15, 19, 22, 23, occludin, or zonula occludens 1) with the exception of claudin 11, which demonstrates significant age-dependent transcript fluctuation (Supplementary Data 1, sheet S1). Claudin 1 displayed a tendency towards an increased expression in the 24 M old rats (Supplementary Data 1), which was replicated at the protein level (Supplementary Fig. S2a).

None of the transport mechanisms usually assigned to CSF secretion[33] appeared amongst the membrane transport mechanisms differentially expressed across the age groups (Fig. 4b). We therefore extracted this set of transport proteins to determine their age-dependent distribution (Fig. 4c). Although several of these, the $Na^+,K^+,2Cl^-$ cotransporter 1 (NKCC1), the Cl^-/HCO_3^- exchanger 2 (AE2), the Na^+/K^+-ATPase α1, the Na^+-coupled HCO_3^- transporters NBCe2 and NCBE, but not aquaporin 1 (AQP1), displayed a tendency to increase from the 1 month age group to the 3 months age group, none declined significantly with old age (Fig. 4d), confirmed at the protein level with the Na^+/K^+-ATPase, the NKCC1, and AQP1 (Fig. 4e and Supplementary Fig. S2b–d). With such stable expression of the transport proteins involved in CSF secretion, we speculated that the metabolism required to sustain the secretory apparatus remained high throughout the rat life span. To determine the age-dependent gene expression of genes involved in metabolism, we extracted the biological function of the differentially expressed genes with enrichment analysis (Supplementary Fig. S3a and Supplementary Data 1, sheet S2). The 1072 differentially expressed genes were assigned to 2306 biological functions, meaning that some genes appear in more than one category, with 489 genes (21%) remaining unclassified. The most abundant category in the enrichment plot was 'cellular processes' (534 genes, 23%), followed by 'biological regulation' (292 genes, 13%) and 'metabolic processes' (281 genes, 12%) (Supplementary Fig. S3a). The 281 differentially expressed genes encoding metabolic processes displayed a significant decline from the 1-month-old rats to the rest of the age groups, with no significant fluctuations in the rest of the age groups (Supplementary

Fig. S3b). The genes involved in glycolysis (listed in Supplementary Data 1, sheet S3) displayed a tendency towards a decline in expression level from the rats of 1 month to those of 3 months of age, and again from the 18-month-old rats to the 24-month-old ones (Supplementary Fig. S3c). In contrast, the genes encoding enzymes involved in the TCA cycle (listed in Supplementary Data 1, sheet S3) were significantly upregulated in the 12-month-old rats, followed by a significant down-regulation in the 18-month-old rats, and a return to baseline by 24 months of age (Supplementary Fig. S3d).

The choroid plexus sustains its high metabolic rate throughout aging

To elucidate the age-dependent metabolic function of the choroid plexus, we performed stable isotope tracing on the acutely excised choroid plexus (Fig. 5a, b). Initially, we determined the metabolic capacity of the lateral choroid plexus compared to other tissues, including the cerebral cortex, muscle, and other epithelial tissues (proximal tubule and small intestine) in the 3-month-old rats (Fig. 5c). ^{13}C enrichment from metabolism of $[U-^{13}C]$glucose was robustly detected in aspartate, citrate, malate and succinate across the five different tissues. We found that the cycling ratios were significantly higher in the lateral choroid plexus compared to the other tissues with a cycling ratio for e.g., citrate in choroid plexus of 3.75 ± 0.11, in the cerebral cortex of 0.95 ± 0.12, in the small intestine of 1.29 ± 0.08, in the muscle of 0.92 ± 0.14, in the proximal tubule of 1.29 ± 0.10, $n = 6$-7, $P < 0.05$ (Fig. 5c). The metabolic activity of the different tissues was similarly distributed irrespective of the quantified metabolite (Fig. 5c) and averaged across all four quantified metabolites, the metabolic activity of choroid plexus was 3.8-fold higher than cerebral cortex, 2.5-fold higher than small intestine, 2.6-fold higher than muscle and 2.1-fold higher than proximal tubule. The choroid plexus thus displays an exceedingly high baseline activity of the TCA cycle, both regarding the lateral choroid plexus (Fig. 5c) and the fourth choroid plexus (Supplementary Fig. S4a). To then determine whether healthy ageing affects the high metabolic activity of the choroid plexus, we quantified $[U-^{13}C]$glucose metabolism in the acutely excised choroid plexus from rats of 1, 3, 6, 12, 18 and 24 months of age (Fig. 5d). The 1-month-old rats displayed a slightly higher metabolic activity of the choroid plexus compared to some of the groups of older rats, when compared across all tested metabolites (Fig. 5d), e.g., the cycling ratio of citrate was 4.09 ± 0.08 in the 1 M rats, compared to 3.56 ± 0.09 in the 3 M rats, $P < 0.05$, 3.54 ± 0.16 in the 6 M old rats, $P < 0.05$, 3.73 ± 0.16 in the 12 M old rats, $P = 0.32$, 3.39 ± 0.12 in the 18 M old rats, $P < 0.05$, and 3.60 ± 0.11 in the 24 M old rats, $P = 0.70$, $n = 6$ of each group (Fig. 5d). This pattern was also observed for the fourth choroid plexus (Supplementary Fig. S4b). However, there was no significant decline of the metabolic activity from 3-months-old to any of the older groups of rats (Fig. 5d), suggesting that the high metabolic activity of the choroid plexus is sustained throughout ageing.

Aging choroid plexus retains mitochondrial morphology and function

Due to the maintenance of high metabolic activity throughout aging, our attention was drawn to mitochondria, which are important for sustaining the energy required for the activity of the choroid plexus epithelial cells. Ultrastructural images revealed no significant changes in mitochondrial morphology between the different age groups (Fig. 6a). In fact, neither mitochondrial density ((mitochondria/100 μm^2) 1 M: 9.55 ± 0.75; 3 M: 7.66 ± 0.61; 6 M: 8.25 ± 0.67; 12 M: 8.83 ± 1.20; 18 M: 8.00 ± 0.43; 24 M: 9.99 ± 1.76, $n = 3$, Fig. 6b), overall cross-sectional area ((in μm^2/cell) 1 M: 0.71 ± 0.01; 3 M: 0.80 ± 0.06; 6 M: 0.70 ± 0.01; 12 M: 0.76 ± 0.05; 18 M: 0.70 ± 0.03; 24 M: 0.74 ± 0.05, $n = 3$, Fig. 6c), nor shape, as measured by circularity (1 M: 0.84 ± 0.01; 3 M: 0.84 ± 0.01; 6 M: 0.85 ± 0.01; 12 M: 0.83 ± 0.01; 18 M: 0.84 ± 0.01; 24 M: 0.84 ± 0.01, $n = 3$, Fig. 6d), showed any statistical differences through aging. Mitochondrial function was then determined by oxidative phosphorylation capacity of
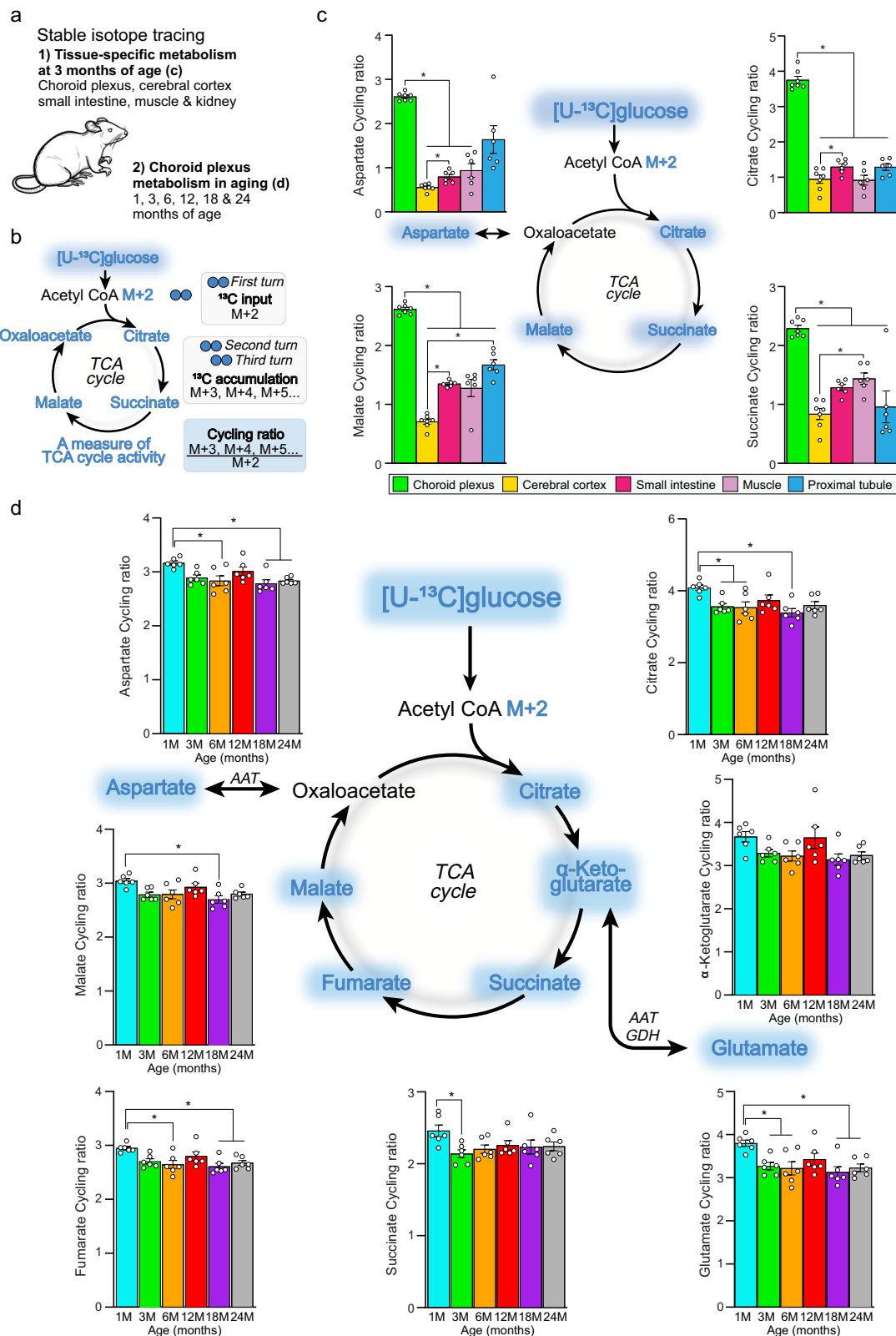
Fig. 5 | Metabolic activity of choroid plexus as a function of age. a Stable isotope tracing was used to assess the metabolic activity of choroid plexus compared to other tissues (**c**) and as a function of age (**d**). **b** Oxidative [U-^{13}C]glucose metabolism was determined by the cycling ratio being a relative measure of tricarboxylic acid (TCA) cycle activity. **c** Tissue-specific metabolic activity of lateral choroid plexus (3 M rats, *n* = 6 (small intestine (dark pink), skeletal muscle (pink), proximal tubule (blue)) or 7 (choroid plexus (green), cerebral cortex (yellow)) rats). **d** Metabolic activity of lateral choroid plexus as a function of age (*n* = 6 rats in age group). 1 M; turquoise, 3 M; green, 6 M; orange, 12 M; red, 18 M; purple, 24 M; grey. Data are presented as mean ± SEM, and statistical significance was tested with one-way ANOVA followed by Tukey's multiple comparisons test. Asterisks denote statistical significance (*P < 0.05). Non-significance is not illustrated for clarity. Source data are provided as a Source Data file and exact *P*-values in Supplementary Data 2.
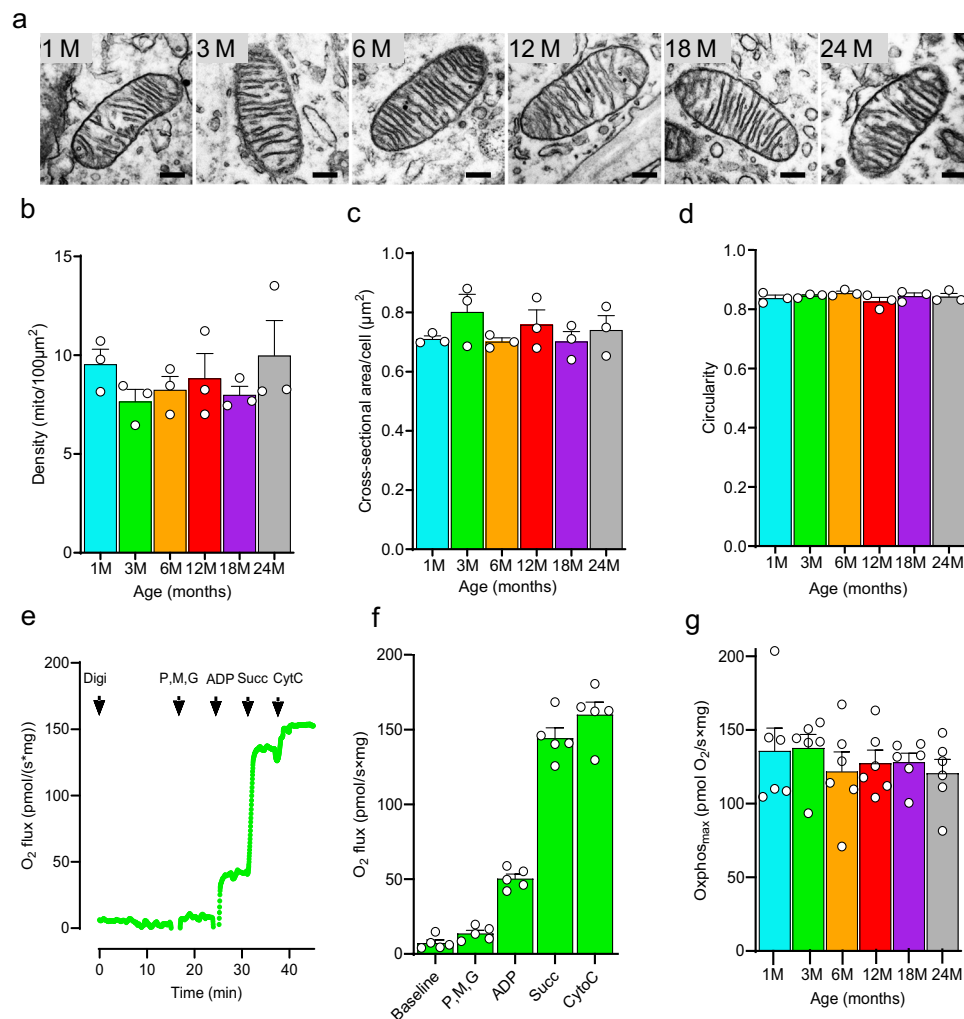
Fig. 6 | **Mitochondrial morphology and functional capacity of the choroid plexus as a function of age. a** Representative TEM images of mitochondria at all ages. Scale bar: 200 nm. Quantification of mitochondrial (mito) density (**b**), cross-sectional area (**c**), and circularity (**d**), $n = 3$ rats (each dot represents the average of seven images per animal). **e** Representative trace of oxygen consumption (O_2 flux, reported per mg choroid plexus tissue) in the lateral choroid plexus from a 3 M rat with compound additions marked with arrows. **f** Steady state O_2 flux in 3 M rat following each compound addition (as illustrated in panel **e**), $n = 5$. **g** Maximal oxidative phosphorylation capacity (Oxphos$_{max}$) of choroid plexus as a function of age, $n = 6$ of each. Digi; digitonin, P; pyruvate, M; malate, G; glutamate, Succ; succinate, CytC; cytochrome C. 1 M; turquoise, 3 M; green, 6 M; orange, 12 M; red, 18 M; purple, 24 M; grey. Data are presented as mean ± SEM and statistical significance was tested with Kruskal-Wallis test followed by Dunn's multiple comparisons test (**b**–**d**) or with one-way ANOVA followed by Tukey's multiple comparisons test (**f**, **g**). Non-significance is not illustrated for clarity. Source data are provided as a Source Data file.

the choroid plexus, measured with high-resolution respirometry. Initially we resolved the oxidative phosphorylation capacity of choroid plexus acutely excised from 3-months-old rats by quantifying the O_2 flux in response to sequential titration of various electron transport chain substrates (Fig. 6e, f). The maximal oxidative phosphorylation capacity, represented by the ΔO_2 flux between baseline and succinate titration, amounted to 137 ± 8 pmol/s×mg, $n = 5$. Mitochondria outer membrane integrity was verified following quantification of the percentile increase in O_2 flux upon the addition of cytochrome C, $10.9 \pm 2.5\%$, $n = 5$, which contributes validation of adaptability of the assay to choroid plexus. The maximal oxidative phosphorylation capacity was stable across all age groups ((in pmol/s×mg): 1 M: 135 ± 15; 3 M: 138 ± 9; 6 M: 122 ± 13; 12 M: 127 ± 9; 18 M: 128 ± 6; 24 M: 121 ± 9, $n = 6$ of each, $P = 0.83$) with no statistically significant reduction with aging (Fig. 6g).

Discussion

We here demonstrate that male rats generally retain their choroid plexus structure and function with age and thus display stable CSF dynamics in aging. Young rats had significantly larger relative brain weight and higher brain water content than their aged counterparts, the latter of which is also evident in infants and young children[34]. The rats displayed reduced total brain water content with aging, although stabilizing around 12 months of age. Brain water content represents all fluid-containing cells and (interstitial) compartments in the brain, with the CSF surrounding the brain lost during brain isolation. Our data therefore do not reflect the general ventricular enlargement generally observed with age-dependent brain atrophy in both rats and humans with aging[21,35,36]. The young rats displayed a tendency towards a lower ICP, but no significant changes observed across the age groups, which is in line with earlier reports on aging human subjects[37–39], but contrasting a proposed age-related reduction of human ICP[40]. The resistance to CSF outflow, likewise, remained constant across age groups, suggesting that the CSF drainage capacity is intact also in aged rats, aligning with earlier studies on healthy human subjects suggesting either no, or a slight, increase in the resistance to outflow with age[37,39]. Of note, this type of analysis measures the ease by which an experimentally-induced excess of brain fluid is cleared from the CSF system, irrespective of the mechanism of CSF absorption and the anatomical location, and therefore reflects the capacity for CSF

drainage, rather than rate of drainage in the resting state. The latter manifests in an age-dependent reduction of CSF outflow via the basal meningeal lymphatic vessels or across the cribriform plate to the lymphatic vessels, as determined with a fluorescent indicator, in mice[41–43] and in rats until the 12 months age, after which the drainage stabilized[44].

The CSF secretion rate in the anesthetized rats increased after the 1 month of age, in accordance with an earlier study[45], but remained constant in the remaining life span of the rat (with the exception of a small increase at 18 M with a subsequent decline at 24 M, at which time point the CSF secretion rate was similar to that of the 3-12 M). Of note, aged rats used for this study did not show overt neurological symptoms, but their cognitive status was not tested prior to experiments. Chiu et al.[21] reported an increased CSF secretion rate from 3-month-old rats to the older age groups, with a constant CSF secretion rate from 12 to 20 months of age, in accordance with the present study. Their 30-month age group displayed a decline in the CSF secretion rate, which could suggest an age-dependent decrease in CSF secretion rate in very old rats, a tendency we also observed in our oldest age group (24 M), which could be the beginning of a very-old-age-dependent decline. The discrepancy could thus reside in the 6 months age difference (6 months older than our oldest rats at 24 months), the different rat strain (F344/BN hybrid) employed, or critical differences in animal ventilation during the procedures. In particular, Chiu et al. did not implement mechanical ventilation, and this may have affected the old age group. We, in fact, quickly noticed that the 24-month-old rats required swift initiation of assisted ventilation following anesthesia to ensure proper physiological blood parameters and hence survival. This age-dependent requirement for mechanical ventilation prevented the use of the alternative 'direct method' to assess CSF secretion rate[46]. To avoid such confounding elements, the CSF secretion measurements could therefore be conducted in awake rats, as was recently demonstrated to provide larger CSF secretion rates than during anesthesia[46]. In mice, the CSF secretion rate was reported slightly reduced in aged mice, but remained rate stable in all preceding age groups[22]. Earlier studies in goats revealed an age-dependent reduction in fluid exiting the in situ perfused choroid plexus in anesthetized goats[16]. This reduction was, however, countered by an age-dependent increase in choroid plexus weight (as also observed in humans[47,48]), which, taken together, suggests a constant CSF secretion rate in aging goats. Although one study suggested an age-dependent reduction of the CSF secretion rate in healthy humans by a modified Masserman technical approach[23], and another suggested an increased CSF secretion rate by determination of CSF protein content[18], several phase contrast magnetic resonance imaging (MRI) studies performed on human subjects demonstrate either no difference[17] or age-dependent either elevation[19,20] or reduction[24,25] of the aqueductal CSF flow. The MRI-based CSF flow quantifications are, amongst other factors, influenced by the arterial pulsation, which also changes with age[24], and may, in addition, depend on the aqueductal diameter. Taken together, it remains unresolved to what extent (or if) the CSF secretion rate, on a general basis, alters with healthy aging. Of note, with the larger total CSF volume in aged humans and rodent[21,35,36], undisturbed rates of CSF secretion and drainage will lead to reduce combined CSF turnover. The estimated doubling of the total CSF volume between 3 M and 24 M of age, as reported for F344/BN rats[21], is thus predicted to half the CSF turnover rate and thereby slow clearance of metabolites and toxins. Such reduced clearance of waste products could contribute to turning physiological aging into neurodegenerative disease. With the numerous reports of altered choroid plexus volume, morphology, and transcriptomics or blood-choroid plexus-CSF barrier function in various neurodegenerative diseases, such as multiple sclerosis, Alzheimer's disease, amyotrophic lateral sclerosis, and Parkinson's disease[49–55], one may anticipate future elucidation of alterations in this system as contributing factors in occurrence of neurodegenerative pathology.

The sustained CSF secretion/K capacity in aging rats aligns with the strikingly unchanged lateral choroid plexus morphology in the aging rats, where the epithelial cells remained cuboidal with identical cross-sectional area, microvilli length and abundance, and tight junctional coupling. The age-persistent tight junctional coupling corroborates a previous demonstration in rats of a different species; Sprague-Dawley[56], with earlier reporting of either a similar maintenance of microvilli coverage[13], or slightly shorter, but denser microvilli with aging in this strain of rats[56]. Murine and human choroid plexus epithelial cells flatten with age[12,14], with a slight shortening of the microvilli length in the aging mouse choroid plexus. Aged murine choroid plexus displayed reduced tight junctional contact area[12], although with no general reduction in transcripts encoding tight junctional proteins in aged mice[57]. The latter aligned with the aging rats in the present study, which displayed no overall reduction in transcripts encoding junctional proteins, nor in individual transcript abundance of the expressed tight junctional proteins, with the exception of claudin 11, demonstrating a significant age-dependent transcript fluctuation. Taken together, there may be species- and strain-dependent differences in choroid plexus morphology in aging although direct functional effects of the reported age-dependent changes await future quantification. In addition, age-related degradation or modification of relevant choroid plexus transport proteins or tight junction proteins, as observed for claudin 1[57], are likely to affect choroid plexus function with aging, although claudin 1 remained stable at the protein level in the aging rats here employed. Lastly, with the different localization, gene transcription, and developmental profiles[58,59] of the choroid plexuses in the lateral ventricles versus the one in the fourth ventricle, the latter could well age differently from those placed in the lateral ventricles of the forebrain.

Transcriptomic analysis of the aging choroid plexus revealed a notable clustering of the young rats (1 M) versus the adult rats (3 M, 6 M, 12 M), which again were distinct from that of the old rats (18 M, 24 M), suggesting age-dependent gene expression in the rat choroid plexus, as previously reported for mice and humans[58,60]. Nevertheless, the groups shared expression of the vast majority of genes, with only ~1000 genes differentially expressed over the different age groups. Of note, it is possible that larger sample sizes could highlight small differences not detectable in a three-sample size experiment. The choroid plexus from young rats displayed the largest number of exclusive transcripts, which aligned with most of the assigned molecular functions of the differentially expressed genes being elevated in this young age group. Of the differentially expressed genes, 7% were assigned to the protein class of transporters, of which we observed no general age-dependent reduction in expression of transporters involved in the clearing of brain waste product and toxins. However, the abrupt decline of transcripts encoding nucleoside and peptide transporters at 24 M may likely affect neuronal homeostasis and maintenance and could thus influence neuronal function with aging. Transcripts encoding the transport proteins that are generally considered implicated in CSF secretion remained stable with aging, which aligns with the stable CSF secretion rates observed in all age groups in the present study. We confirmed the stable expression at the protein level for the Na^+/K^+-ATPase, the NKCC1, and the AQP1, although the latter displayed a tendency towards higher levels in the middle-aged (6-18 M) groups. With the recent demonstration of AQP1 not required for CSF secretion[61], such potential decline is not expected to influence CSF secretion in aging. We cannot exclude altered abundance of the transporters not tested at the protein level, nor age-dependent changes in their potential post-translational modifications, which could, together or alone, affect the protein activity level. Accordingly, earlier studies on aged choroid plexus have demonstrated either constant expression of the Na^+/K^+-ATPase in mice[12] or apparently reduced (although unquantified) immunodetection of the Na^+/K^+-ATPase in Sprague-Dawley rats[56],

which contrasts the stable protein level of Na⁺/K⁺-ATPase in aging rats here observed.

Twelve percent of the differentially regulated genes belonged to the protein class of metabolic processes. These genes, and those involved in both glycolysis and the TCA cycle, were generally reduced in transcript abundance from the 1-month-old rats, but remained stable across the remaining age groups. These transcriptomic findings were reflected in the metabolic rate of excised choroid plexus, which, likewise, was reduced after 1 month of age, but remained intact throughout aging in both choroid plexus of the lateral ventricle and that of the fourth ventricle. The choroid plexus metabolism was ~4-fold higher than the cerebral cortex and ~2.5-fold higher than muscle tissue and two other fluid-transporting epithelia (proximal tubule and small intestine), underscoring the high metabolic requirement for sustenance of the CSF production in addition to the multitude of other functions served by the choroid plexus. Curiously, this age-resistant metabolic rate is not mirrored in cortical tissue, with its well-established metabolic decline with age in humans, mice and rats[62–64], suggesting the importance of sustained CSF secretion in the aging brain. Lastly, mitochondrial function, as determined by their capacity for oxidative phosphorylation, also remained stable across lateral choroid plexuses from the different age groups, with no indication of declined mitochondrial activity in aged rats. These findings align with the observed integrity of mitochondrial morphology, cross-sectional area, and density across the age groups. The intact oxidative phosphorylation capacity of aged mitochondria mirrors that observed in murine choroid plexus, despite their elongation with age[12].

In conclusion, male rats retain their capacity for CSF absorption and secretion throughout healthy aging, which aligns with the morphologic, transcriptomic, and metabolic stability of the choroid plexus epithelium in the tested time span. Future research should address putative sex-specific differences in healthy aging of the CSF secretion machinery and CSF dynamics. Although some data sets may indicate a similar functional stability in larger mammals, including humans, neurodegenerative pathologies e.g., Alzheimer's disease may be associated with reduced CSF secretion and/or CSF turnover[5,18,26,65], which could contribute to slower clearance of metabolites and toxic compounds and thus worsened cognition. Future determinations of neuropathology-related disturbances in CSF dynamics should, however, consider that rodent models generally fail to fully recapitulate neurodegenerative pathologies such as Alzheimer's disease. Nevertheless, an improved understanding of CSF dynamics in health versus diseased aging may pave the way towards uncovering whether manipulation of the CSF secretion apparatus could prove beneficial in the treatment of neurodegenerative diseases associated with reduced waste clearance and cognitive decline[5].

Methods

Experimental rats
All animal experiments conformed to the European guidelines and ethical regulations for the use of experimental animals. The experiments were approved by the animal facility at the Faculty of Health and Medical Sciences, University of Copenhagen, and by the Danish Animal Experiments Inspectorate (permission number 2021-15-0201-00867). Male Wistar rats (Janvier) of ages 1, 3, 6, 12, 18, and 24 months were employed in the study. The rats were housed with 12:12 light cycle with access to water and food *ad libitum* in accordance with the guidelines of the Danish Veterinary and Food Administration (Ministry of Environment and Food). When possible, several experiments were performed on the same rats in order to reduce the number of experimental animals, i.e., the bodyweight and brain weights (Fig. 1) were determined from one set of rats, of which the choroid plexuses were extracted from the brains for RNAseq (Figs. 3–4) prior to determination of brain water content (Fig. 1), the intracranial pressure (ICP) was recorded just prior to the resistance to outflow determination in another set of rats (Fig. 1), and the choroid

plexuses for electron microscopy (Figs. 2,6) were extracted after termination of the ventriculo-cisternal perfusion assay (Fig. 1).

Anesthesia and physiological parameters
The experimental rats were anaesthetized with intraperitoneal (i.p.) administration of xylazin and ketamine (ScanVet, 10 mg/kg animal xylazine, 5 min later 100 mg/kg animal ketamine, half dose of ketamine was re-dosed every 10–40 min upon detection of foot reflex). The body temperature of the anesthetized rats was maintained at 37 °C by a homeothermic monitoring system (Harvard Apparatus). Mechanical ventilation was included for anesthetic protocols longer than 30 min to ensure stable respiratory partial pressure of carbon dioxide and arterial oxygen saturation, and thus stable plasma pH and electrolyte content. A surgical tracheotomy was performed and the ventilation controlled by the VentElite system (Harvard Apparatus) by 0.9 l min⁻¹ humidified air mi−xed with 0.1 l min⁻¹ O₂ adjusted with approximately 3 mL/breath, 80 breaths/min, a Positive End-Expiratory Pressure (PEEP) at 2 cm, and 10% sigh for a ~400 g rat. The ventilation settings were optimized for each animal using a capnograph (Type 340, Harvard Apparatus) and a pulse oximeter (MouseOx® Plus, Starr Life Sciences) after system calibration with respiratory pCO₂ (4.5–5 kPa), pO₂ (13.3–17.3 kPa), and arterial oxygen saturation (98.8–99.4%) (ABL90, Radiometer). The eldest group of rats (24 months of age) was generally more sensitive to the anesthetic agents, and respiration momentarily stopped in some of the rats before the insertion of the tracheal ventilation tube. Mechanical ventilation of the rats, however, ensured stable heart rates (Supplementary Fig. S5a) and ensured oxygen saturation in all age groups during the experimental time window, albeit with an age-dependent reduction in baseline heart rate (Supplementary Fig. S5b).

Determination of brain water content
The rat brain was swiftly removed following anesthesia and decapitation, placed in a pre-weighed porcelain evaporating beaker (Witeg), and weighed within minutes after brain isolation. The brain tissue was dried at 100 °C for 72 h to a constant mass. The dry brain was weighed, and the brain water content was determined in mL/gram dry weight using the equation: (wet weight - dry weight)/dry weight.

CSF production rate
(Equation 1). The CSF production rate was determined with the ventriculo-cisternal perfusion technique. A 4 mm brain infusion cannula (Brain infusion kit 2, Alzet) was stereotaxically placed in the right lateral ventricle of an anesthetized and ventilated rat (coordinates: 1.3 mm posterior to Bregma, 1.8 mm lateral to the midline, and 0.4-0.8 mm ventral), through which pre-heated (37 °C, SF-28, Warner Instruments) HCO₃⁻-buffered artificial CSF (HCO₃⁻-aCSF; (in mM) 120 NaCl, 2.5 KCl, 2.5 CaCl₂, 1.3 MgSO₄, 1 NaH₂PO₄, 10 glucose, 25 NaHCO₃, pH adjusted with 95% O₂/5% CO₂) containing 0.5 mg/mL TRITC-dextran (tetramethylrhodamine isothiocyanate-dextran, MW = 150,000; T1287, Sigma) was perfused at 9 µl/min. CSF was sampled continuously through a glass capillary inserted into another glass capillary inserted into cisterna magna, which prevents elevation of the ICP during the procedure. The outer glass capillary was replaced at 5 min intervals and the fluorescent content of each of these CSF samples was measured in a microplate photometer (545 nm, Synergy™ Neo2 Multi-mode Microplate Reader; BioTek Instruments), and the production rate of CSF was calculated from the equation:

$$V_p = r_i * \frac{C_i - C_o}{C_o} \tag{1}$$

where V_p = CSF production rate (µl min⁻¹), r_i = infusion rate (µl min⁻¹), C_i = fluorescence of inflow solution, C_o = fluorescence of outflow solution, calculated based on the stable time interval from 45-90 min after initiation of the experiment. As earlier demonstrated for young

rats[31], lack of penetration of the dextran across the ependymal lining into the parenchyma was verified following completion of full experiments in both young (3 M) and aged (24 M) old rats (Supplementary Fig. S5c-d).

ICP and resistance to outflow measurements

Anesthetized and ventilated rats were placed in a stereotactic frame and the skull was exposed. A brain infusion cannula (Brain infusion kit 2, Alzet) was placed in the left lateral ventricle (coordinates: 1.3 mm posterior to bregma, 1.8 mm lateral to the midline, 0.4–0.8 mm ventral). After cementing the cannula in place, a 3.6 mm diameter cranial window was drilled in the contralateral side (coordinates: 6 mm posterior to bregma, 1 mm lateral to the midline) with care not to damage the dura. An epidural probe (PlasticsOne, C313G) was secured with dental resin cement (Panavia SA Cement, Kuraray Noritake Dental Inc.) above the dura and the ICP probe was filled with HEPES-aCSF ((in mM) 120 NaCl, 2.5 KCl, 2.5 CaCl$_2$, 1.3 MgSO$_4$, 1 NaH$_2$PO$_4$, 10 glucose, 17 Na-HEPES, adjusted to pH 7.4 with NaOH) prior to connection to a pressure transducer APT300 and transducer amplifier module TAM-A (Hugo Sachs Elektronik) followed by a multifunction data acquisition module DT9836-12-2-BNC (Data Translation). To ensure the presence of a continuous fluid column between the dura and the epidural probe, approximately 5 μl HEPES-aCSF was injected through the epidural probe. The ICP signal was recorded at a 1 kHz sampling rate using BDAS Basic Data Acquisition Software (Hugo Sachs Elektronik). Jugular compression was applied to confirm proper ICP recording. Continuous ICP recordings were performed for at least 20 minutes (and employed for quantification of the age-dependent ICP) before beginning the resistance to CSF outflow assay. Following the baseline ICP measurements, pre-heated (37 °C, SF-28, Warner Instruments) aCSF was infused into the left lateral ventricle through the Alzet for intervals of 10 minutes at 5, 10 and 15 μl/min. (Eq. 2)

Resistance to drainage (R$_{out}$) was calculated using the following equation (derived from[66]):

$$R_{out} = \frac{ICP_{inf} - ICP_{base}}{V_{inf}} \qquad (2)$$

Where ICP$_{inf}$ is the mean ICP of the last three minutes of infusion at a given rate (in mmHg), ICP$_{base}$ is the initial stable ICP baseline the last five minutes before the initiation of the R$_{out}$ measurements (in mmHg), and V$_{inf}$ is the infusion rate (in μl/min). R$_{out}$ for each rate of infusion was calculated and averaged across all infusion rates for each rat to determine resistance to CSF drainage.

RNAsequencing (RNAseq)

Choroid plexuses (from lateral and fourth ventricles) were isolated from the anesthetized and decapitated rat and stored in RNAlater® (Sigma-Aldrich, St. Louis, Missouri, USA) at −80 °C. The RNA extraction and library preparation were performed by Novogene Company Limited, UK, with NEB Next® Ultra™ RNA Library Prep Kit (NEB, USA) prior to their RNA sequencing (paired-end 150 bp, with 12 Gb output) on an Illumina NovaSeq 6000 (Illumina, USA). The 150 base-pair end reads were mapped to the reference genome (Rattus norvegicus Rnor_6.0 v.104) using Spliced Transcripts Alignment to a Reference (STAR) RNA-seq aligner (v. 2.7.9a)[67]. The data was normalized using DEseq2 (v. 3.16)[68] using standard procedure[69]: The gene expression was normalized for ranking of gene expression to trimmed mean of M-values (TMM)[70] by 'conorm' python library (v.1.2.0) (https://pypi.org/project/conorm/). A density plot was generated using DEseq2[68] normalized data Median Ratio Normalization (MRN)[69]. A principal component analysis (PCA) was generated using DEseq2 rlog transformed data, Relative Log Expression (RLE), utilizing Scikit-learn python library[69,71]. The Venn diagram was generated

using TMM normalized data, excluding genes expressed below 10 TMM, utilizing R library 'venn' and 'ggplot2'[72,73]. The genes shared between the age groups are displayed in the venn diagram in a binary manner (present if expressed above the threshold). All three data normalization methods were compared and yielded virtually identical results, with no discernible impact on downstream analyses. Differential expression of genes between age groups was determined based on DEseq2 Likelihood Ratio Test (LRT)[68]. These differentially expressed genes were employed for the subsequent bioinformatics analyses. The differentially expressed genes were categorized by their three major gene ontology terms 'Molecular function', 'Protein classes', and 'Biological function'[74,75] by utilizing the PANTHER database (accessed 8 Sep 2023)[76,77]. The gene symbols were gathered from the Ensembl Biomart extension (accessed 8 Sep 2023)[78,79] and used as input for the PANTHER database. The gene annotation obtained from the PANTHER gene lists of the subcategories within 'Molecular function', 'Protein classes', and 'Biological function' was mapped back to Ensembl ID using 'gene symbol' and 'UniProt IDs' as reference. The ensembl IDs without reference to a 'gene symbol' in the PANTHER database was annotated 'Unclassified'. A 'small group collection' was implemented for the enrichment plots containing groups of 'Molecular function' and 'Biological function' less than one percent, and 'Protein classes' less than two percent. Time series plots were generated using DEseq2 normalized (MRN) data transformed to z-score. The table of transport mechanisms was generated using DEseq2 normalized data (MRN) transformed to z-score and ranked according to normalized mean TMM values across all samples. Genes encoding transporters involved in neuroprotection and efflux were selected based on the gene list from Kratzer et al.[32]. All program parameter settings for library building and mapping, and libraries/packages, together with all scripts for the gene annotation and analysis are available at https://github.com/Sorennorge/MacAulayLab-Age-Study. Raw data are available at the National Center for Biotechnology Information (NCBI) Gene Expression Omnibus (GEO) database (accession number: GSE246313).

Western blotting

Rats were anesthetized, decapitated, and the brains removed and immersed in ice-cold HEPES-aCSF for 10 min before isolation of the lateral choroid plexuses. Two isolated lateral choroid plexuses *per* rat were lysed in 90 μl RIPA buffer (in mM: 150 NaCl, 50 Tris pH 8.0, 5 EDTA, 0.5% sodium deoxycholate, 0.1% SDS and 1% Triton X-100; Sigma) supplemented with the protease inhibitors pefabloc (0.4 mM, Sigma-Aldrich) and leupeptin (8 μM, Sigma-Aldrich), sonicated (70% power for 3 ×5 secs intervals, Sonopuls, Bandelin), and centrifuged at 13.000 × g for 3 min at 4 °C. 30 μl sample buffer (4% SDS, 0.006% Bromphenol Blue, 8.7% glycerol, 0.25% Tris-base and 0.75% DTT, pH 6.8, adjusted with HCl) was added, the samples were heated up to 65 °C for 10 min and stored at −80 °C. Of the lysed choroid plexus, we loaded 10 μl (Na$^+$/K$^+$-ATPase) or 12 μl (claudin 1) on precast SDS-PAGE gels (4–20% Criterion TGX, Bio-Rad) and transferred using immobilon-FL membranes (Merck Millipore). The membranes were blocked in Odyssey blocking buffer PBS (LI-COR) and probed with primary antibodies: mouse anti-Na$^+$/K$^+$-ATPase α1 a6F (1:60, a6F, DSHB), rabbit anti-claudin-1 (1:1000, ab307692, Abcam), rabbit anti-AQP1-1 (1:1000, ab307692, Alomone), sheep anti-NKCC2 (2 μg/ml, S022D, Dundee University), and as a loading control; chicken anti-GAPDH (1:800, AB2302, Millipore), all diluted in blocking buffer:PBS-T 1:1. Primary antibodies were detected using fluorophore-conjugated secondary antibodies (all 1:10.000; IRDye 680RD Donkey anti-chicken, IRDye 800CW Goat anti-mouse; IRDye 800CW Goat-anti rabbit, rabbit anti sheep IgG, DyLight

800 conjugate, LI-COR) and scanned on an Odyssey CLx imaging system (Image Studio ver. 5.2, LI-COR). Image analysis was performed using Image Studio software (LI-COR).

Transmission Electron Microscopy (TEM)

Choroid plexuses of the lateral ventricles were isolated from anesthetized and decapitated rats and fixed in 2% v/v glutaraldehyde in 50 mM sodium phosphate buffer (pH 7.2) at 4 °C until further processing. Following a phosphate buffer (0.2 M) wash, the choroid plexus underwent post-fixation in a 1:1 mixture of 2% aqueous osmium tetroxide (Electron Microscopy Sciences, Hatfield, PA) and 3% potassium ferrocyanide (Sigma-Aldrich) at 4 °C for 1 hour. It was then dehydrated in increasing acetone concentrations (30%, 60%, 90%, 100%) for 15 min each. The samples were subsequently incubated in acetone/Spurr resin (1:1 for 30 min, then 1:2 for 30 min) and left in Spurr resin (Electron Microscopy Sciences) overnight at room temperature. The choroid plexuses were embedded in Spurr resin within capped 00 BEEM capsules (Electron Microscopy Sciences) for 24 h at 70 °C. An ultramicrotome (EM UC6, Leica Microsystems) was used to cut ultrathin sections (70 nm), which were collected on uncoated nickel grids (100 mesh). These sections were counterstained with UranyLess EM Stain for 30 s and lead citrate (both from Electron Microscopy Sciences) for 30 s. A JEM-1400 Flash transmission electron microscope (JEOL, Tokyo, Japan) was utilized to examine the sections. The Jeol Matataki Flash camera's automated montage system was employed to obtain electron micrographs. The lateral choroid plexus from three different animals from each age group was imaged and seven images from each choroid plexus were chosen for quantification (in total 21 images per age group). Cells were selected such that both apical and basal compartments and lateral borders were visible. The analysis was performed using ImageJ (Fiji, NIH) with a previously published custom semi-automated macro[12]. The following parameters were analyzed: cross-sectional cell area (μm^2); cell axis ratio, calculated as the proportion between horizontal (distance between the lateral extremities of the cell) and vertical (distance between basal to apical extremities - microvilli not included) lengths; microvilli length (μm), average of three segments measured from the apical border of the epithelial cell until the end of the microvilli (segments were placed at both lateral extremities and the center of the structure); mitochondrial density (mito/μm^2); mitochondrial cross-sectional area (μm^2/cell), computed as the mean area occupied by all mitochondrial profiles in a cell; mean circularity of all mitochondria in a cell, derived using the formula $4\pi \times$ Area/Perimeter^2 (with values near 1 indicating round mitochondrial profiles and those closer to 0 suggesting elongated shapes).

Metabolic mapping using stable isotope tracing

Oxidative glucose metabolism in the tricarboxylic acid (TCA) cycle was determined by ^{13}C isotope tracing[80]. Three-months-old Wistar rats were anesthetized and sacrificed before isolation of the intact lateral and fourth choroid plexuses, small pieces of the cerebral cortex, small intestine, hind leg muscle, and isolated proximal tubule[81]. The tissues were swiftly transferred to oxygenated (5% CO_2/95% O_2) Dulbecco's Modified Eagle's Medium with pH = 7.4 (Sigma-Aldrich, D5030), containing 5 mM [U-^{13}C]glucose and incubated for 30 minutes at 37 °C. The incubation was terminated by transferring the tissue to ice-cold 70% ethanol. The isolated proximal tubules were briefly centrifuged to form a pellet onto which ice-cold 70% ethanol was added. To determine the age-dependent metabolism of choroid plexus, the lateral and fourth choroid plexuses were isolated from rats of 1, 3, 6, 12, 18, and 24 months of age. The tissues were quickly transferred to gas-equilibrated (5% CO_2/95% O_2) aCSF containing (in mM): 128 NaCl, 25 NaHCO$_3$, 3 KCl, 2 CaCl$_2$, 1.2 MgSO$_4$, 0.4 KH$_2$PO$_4$, and 5 mM [U-^{13}C] glucose (pH = 7.4) and incubated for 30 min at 37 °C. The incubation

was terminated by transferring the tissue pieces to ice-cold 70% ethanol. Before analysis, all tissues were sonicated and centrifuged (4000 g x 20 min), and the supernatant was removed and lyophilized. The tissue extracts were analyzed by gas chromatography-mass spectrometry (GC-MS)[82]. Briefly, extracts were reconstituted in water, acidified, extracted twice with ethanol and metabolites derivatized using N-tert-butyldimethylsilyl-N-methyltrifluoroacetamide. Samples were analyzed by GC (Agilent Technologies, 7820 A, J&W GC column HP-5 MS) coupled to MS (Agilent Technologies, 5977E). The isotopic enrichment was corrected for the natural abundance of ^{13}C by analyzing standards containing the unlabeled metabolites of interest. Isotope tracing reveals the fractional ^{13}C enrichment of metabolites, described as M + X, where M is the molecular ion and X is the number of ^{13}C atoms in the molecule[80]. The fractional ^{13}C enrichment depends on the total metabolite amounts, which may vary across tissues and age. To circumvent this, the isotope tracing results are presented as the cycling ratio[83], describing the metabolite accumulation of ^{13}C generated by subsequent turns of the TCA cycle (M + 3, M + 4, M + 5...) relative to the ^{13}C entry into the TCA cycle (M + 2), reflecting the rate of TCA cycling. As the cycling ratio is a measure of ^{13}C accumulation relative to ^{13}C entry into the TCA cycle, it is only dependent on ^{13}C fluxes, which allows for metabolic comparisons across tissues with potentially different metabolite amounts.

Mitochondrial respiration measurements

The age-dependent mitochondrial respiratory capacity was assessed by high-resolution respirometry[84] using the high-resolution Oxygraph-2k (Oroboros, Innsbruck, Austria). Acutely excised lateral choroid plexuses were swiftly blotted on filter paper and weighed on a XS205 DualRange Analytical Balance (Mettler-Toledo AG, Switzerland). The respirometric measurements were performed in duplicate at 37 °C in mitochondrial respiration medium (MiR05: 0.5 mM EGTA, 3 mM MgCl$_2$, 60 mM potassium lactobionate, 20 mM taurine, 10 mM KH$_2$P0$_4$, 20 mM Hepes, 110 mM sucrose and 1 g/l bovine serum albumin (pH 7.1)). The choroid plexus was initially permeabilized by digitonin (1.25 μg/ml, Sigma-Aldrich) for 15 minutes before the sequential addition of the complex I substrates pyruvate (5 mM, Sigma-Aldrich), malate (2 mM, Sigma-Aldrich), and glutamate (10 mM, Sigma-Aldrich) to provide electrons to complex I. The addition of ADP (5 mM, Sigma-Aldrich) promoted the oxygen flux that reflects complex I oxidative phosphorylation capacity. Subsequent addition of the complex II substrate succinate (10 mM, Sigma-Aldrich) allowed maximal oxidative phosphorylation, with electron flow via both complex I and complex II. To test the integrity of the mitochondria outer membrane, cytochrome C (10 μM, Sigma-Aldrich) was titrated into each chamber. A cytochrome C-induced percentile increase in oxygen flux >20% indicated compromised sample integrity. 10 choroid plexuses (of the 82 here employed) surpassed this threshold and were omitted from the subsequent data analysis.

Data analysis and statistics

All data are shown as mean ± SEM, and statistical analyses were carried out with GraphPad Prism (GraphPad Software).

Statistical significance was determined with a parametric or non-parametric tests depending on whether the data was normally distributed calculated with the D'Agostino-Pearson's test. One or two-way ANOVA (parametric) or Kruskal-Wallis (non-parametric) were employed for statistical analysis followed by Tukey's or Dunn's multiple comparisons *post hoc* test, as indicated in figure legends. $P < 0.05$ was considered statistically significant.

Reporting summary

Further information on research design is available in the Nature Portfolio Reporting Summary linked to this article.

Data availability

The datasets used in the current study are available from the corresponding author on request. Source data are provided with this paper. All program parameter settings for library building and mapping, together with all scripts for the gene annotation and analysis are available at https://github.com/Sorennorge/MacAulayLab-Age-Study[85]. Raw RNAseq data are available at the National Center for Biotechnology Information (NCBI) Gene Expression Omnibus (GEO) database (accession number: GSE246313; https://www.ncbi.nlm.nih.gov/geo/query/acc.cgi?acc=GSE246313). Source data are provided with this paper.

References

1. MacAulay, N., Keep, R. F. & Zeuthen, T. Cerebrospinal fluid production by the choroid plexus: a century of barrier research revisited. *Fluids Barriers CNS* **19**, 26 (2022).
2. Cserr, H. F. Physiology of the choroid plexus. *Physiol. Rev.* **51**, 273–311 (1971).
3. Czarniak, N., Kaminska, J., Matowicka-Karna, J. & Koper-Lenkiewicz, O. M. Cerebrospinal fluid-basic concepts review. *Biomedicines* **11**, 1461 (2023).
4. Feliciano, D. M., Zhang, S., Nasrallah, C. M., Lisgo, S. N. & Bordey, A. Embryonic cerebrospinal fluid nanovesicles carry evolutionarily conserved molecules and promote neural stem cell amplification. *PLoS One* **9**, e88810 (2014).
5. Attier-Zmudka, J. et al. Decreased cerebrospinal fluid flow is associated with cognitive deficit in elderly patients. *Front Aging Neurosci.* **11**, 87 (2019).
6. Kress, B. T. et al. Impairment of paravascular clearance pathways in the aging brain. *Ann. Neurol.* **76**, 845–861 (2014).
7. Li, Y. et al. Decreased CSF clearance and increased brain amyloid in Alzheimer's disease. *Fluids Barriers CNS* **19**, 21 (2022).
8. Simon, M. J. & Iliff, J. J. Regulation of cerebrospinal fluid (CSF) flow in neurodegenerative, neurovascular and neuroinflammatory diseases. *Biochim. Biophys. Acta* **1862**, 442–451 (2016).
9. Bothwell, S. W., Janigro, D. & Patabendige, A. Cerebrospinal fluid dynamics and intracranial pressure elevation in neurological diseases. *Fluids Barriers CNS* **16**, 9 (2019).
10. Hochstetler, A., Raskin, J. & Blazer-Yost, B. L. Hydrocephalus: historical analysis and considerations for treatment. *Eur. J. Med. Res.* **27**, 168 (2022).
11. Rubin, R. C., Henderson, E. S., Ommaya, A. K., Walker, M. D. & Rall, D. P. The production of cerebrospinal fluid in man and its modification by acetazolamide. *J. Neurosurg.* **25**, 430–436 (1966).
12. Scarpetta, V. et al. Morphological and mitochondrial changes in murine choroid plexus epithelial cells during healthy aging. *Fluids Barriers CNS* **20**, 19 (2023).
13. Serot, J. M., Foliguet, B., Bene, M. C. & Faure, G. C. Choroid plexus and ageing in rats: a morphometric and ultrastructural study. *Eur. J. Neurosci.* **14**, 794–798 (2001).
14. Shuangshoti, S. & Netsky, M. G. Human choroid plexus: morphologic and histochemical alterations with age. *Am. J. Anat.* **128**, 73–95 (1970).
15. Ferrante, F. & Amenta, F. Enzyme histochemistry of the choroid plexus in old rats. *Mech. Ageing Dev.* **41**, 65–72 (1987).
16. Chen, R. L., Chen, C. P. & Preston, J. E. Elevation of CSF albumin in old sheep: relations to CSF turnover and albumin extraction at blood-CSF barrier. *J. Neurochem* **113**, 1230–1239 (2010).
17. Gideon, P., Thomsen, C., Stahlberg, F. & Henriksen, O. Cerebrospinal fluid production and dynamics in normal aging: a MRI phase-mapping study. *Acta Neurol. Scand.* **89**, 362–366 (1994).
18. Kleine, T. O., Hackler, R., Lutcke, A., Dauch, W. & Zofel, P. Transport and production of cerebrospinal fluid (CSF) change in aging humans under normal and diseased conditions. *Z. Gerontol.* **26**, 251–255 (1993).
19. Sartoretti, T. et al. Sex and age dependencies of aqueductal cerebrospinal fluid dynamics parameters in healthy subjects. *Front Aging Neurosci.* **11**, 199 (2019).
20. Schmid Daners, M. et al. Age-specific characteristics and coupling of cerebral arterial inflow and cerebrospinal fluid dynamics. *PLoS One* **7**, e37502 (2012).
21. Chiu, C. et al. Temporal course of cerebrospinal fluid dynamics and amyloid accumulation in the aging rat brain from three to thirty months. *Fluids Barriers CNS* **9**, 3 (2012).
22. Liu, G. et al. Direct measurement of cerebrospinal fluid production in mice. *Cell Rep.* **33**, 108524 (2020).
23. May, C. et al. Cerebrospinal fluid production is reduced in healthy aging. *Neurology* **40**, 500–503 (1990).
24. Stoquart-ElSankari, S. et al. Aging effects on cerebral blood and cerebrospinal fluid flows. *J. Cereb. Blood Flow. Metab.* **27**, 1563–1572 (2007).
25. Eisma, J. J. et al. Choroid plexus perfusion and bulk cerebrospinal fluid flow across the adult lifespan. *J. Cereb. Blood Flow. Metab.* **43**, 269–280 (2023).
26. Silverberg, G. D. et al. The cerebrospinal fluid production rate is reduced in dementia of the Alzheimer's type. *Neurology* **57**, 1763–1766 (2001).
27. Preston, J. E. Ageing choroid plexus-cerebrospinal fluid system. *Microsc Res Tech.* **52**, 31–37 (2001).
28. Keep, R. F., Hua, Y. & Xi, G. Brain water content. A misunderstood measurement?. *Transl. Stroke Res.* **3**, 263–265 (2012).
29. Heisey, S. R., Held, D. & Pappenheimer, J. R. Bulk flow and diffusion in the cerebrospinal fluid system of the goat. *Am. J. Physiol.* **203**, 775–781 (1962).
30. Steffensen, A. B. et al. Cotransporter-mediated water transport underlying cerebrospinal fluid formation. *Nat. Commun.* **9**, 2167 (2018).
31. Oernbo, E. K. et al. Membrane transporters control cerebrospinal fluid formation independently of conventional osmosis to modulate intracranial pressure. *Fluids Barriers CNS* **19**, 65 (2022).
32. Kratzer, I. et al. Developmental changes in the transcriptome of the rat choroid plexus in relation to neuroprotection. *Fluids Barriers CNS* **10**, 25 (2013).
33. MacAulay, N. Molecular mechanisms of brain water transport. *Nat. Rev. Neurosci.* **22**, 326–344 (2021).
34. Duhaime, A. C. & Rindler, R. S. Special considerations in infants and children. *Handb. Clin. Neurol.* **127**, 219–242 (2015).
35. Courchesne, E. et al. Normal brain development and aging: quantitative analysis at in vivo MR imaging in healthy volunteers. *Radiology* **216**, 672–682 (2000).
36. Matsumae, M. et al. Age-related changes in intracranial compartment volumes in normal adults assessed by magnetic resonance imaging. *J. Neurosurg.* **84**, 982–991 (1996).
37. Albeck, M. J. et al. Age dependency of resistance to cerebrospinal fluid outflow. *J. Neurosurg.* **89**, 275–278 (1998).
38. Czosnyka, M., Czosnyka, Z. H., Whitfield, P. C., Donovan, T. & Pickard, J. D. Age dependence of cerebrospinal pressure-volume compensation in patients with hydrocephalus. *J. Neurosurg.* **94**, 482–486 (2001).
39. Malm, J., Jacobsson, J., Birgander, R. & Eklund, A. Reference values for CSF outflow resistance and intracranial pressure in healthy elderly. *Neurology* **76**, 903–909 (2011).
40. Pedersen, S. H., Lilja-Cyron, A., Andresen, M. & Juhler, M. The relationship between intracranial pressure and age-chasing age-related reference values. *World Neurosurg.* **110**, e119–e123 (2018).
41. Ahn, J. H. et al. Meningeal lymphatic vessels at the skull base drain cerebrospinal fluid. *Nature* **572**, 62–66 (2019).
42. Brady, M. et al. Cerebrospinal fluid drainage kinetics across the cribriform plate are reduced with aging. *Fluids Barriers CNS* **17**, 71 (2020).

43. Ma, Q., Ineichen, B. V., Detmar, M. & Proulx, S. T. Outflow of cerebrospinal fluid is predominantly through lymphatic vessels and is reduced in aged mice. *Nat. Commun.* **8**, 1434 (2017).

44. Nagra, G. & Johnston, M. G. Impact of ageing on lymphatic cerebrospinal fluid absorption in the rat. *Neuropathol. Appl Neurobiol.* **33**, 684–691 (2007).

45. Karimy, J. K. et al. A novel method to study cerebrospinal fluid dynamics in rats. *J. Neurosci. Methods* **241**, 78–84 (2015).

46. Toft-Bertelsen, T. L. et al. The cerebrospinal fluid secretion rate increases in awake and freely moving rats but differs with experimental methodology. *Adv. Sci.* **12**, e2412469 (2025).

47. Alisch, J. S. R. et al. Characterization of age-related differences in the human choroid plexus volume, microstructural integrity, and blood perfusion using multiparameter magnetic resonance imaging. *Front Aging Neurosci.* **13**, 734992 (2021).

48. Eisma, J. J. et al. Deep learning segmentation of the choroid plexus from structural magnetic resonance imaging (MRI): validation and normative ranges across the adult lifespan. *Fluids Barriers CNS* **21**, 21 (2024).

49. Rodrigues, A. B. M., Passetti, F. & Guimaraes, A. C. R. Complementary strategies to identify differentially expressed genes in the choroid plexus of patients with progressive multiple sclerosis. *Neuroinformatics* **23**, 10 (2025).

50. Perera, C. et al. Non-invasive MRI of blood-cerebrospinal fluid-barrier function in a mouse model of Alzheimer's disease: a potential biomarker of early pathology. *Fluids Barriers CNS* **21**, 97 (2024).

51. Sun, S. et al. Elevated peripheral inflammation is associated with choroid plexus enlargement in independent sporadic amyotrophic lateral sclerosis cohorts. *Fluids Barriers CNS* **21**, 83 (2024).

52. Delvenne, A. et al. Involvement of the choroid plexus in Alzheimer's disease pathophysiology: findings from mouse and human proteomic studies. *Fluids Barriers CNS* **21**, 58 (2024).

53. Jiang, J. et al. Choroid plexus volume as a novel candidate neuroimaging marker of the Alzheimer's continuum. *Alzheimers Res Ther.* **16**, 149 (2024).

54. Courtney, Y., Hochstetler, A. & Lehtinen, M. K. Choroid plexus pathophysiology. *Annu. Rev. Pathol.* **20**, 193–220 (2025).

55. Jeong, S. H. et al. Association of choroid plexus volume with motor symptoms and dopaminergic degeneration in Parkinson's disease. *J. Neurol. Neurosurg. Psychiatry* **94**, 1047–1055 (2023).

56. Masseguin, C., LePanse, S., Corman, B., Verbavatz, J. M. & Gabrion, J. Aging affects choroidal proteins involved in CSF production in Sprague-Dawley rats. *Neurobiol. Aging* **26**, 917–927 (2005).

57. Chen, Y. et al. Macrophage-derived CTSS drives the age-dependent disruption of the blood-CSF barrier. *Neuron* **113**, 1082–1097 (2025).

58. Dani, N. et al. A cellular and spatial map of the choroid plexus across brain ventricles and ages. *Cell* **184**, 3056–3074.e3021 (2021).

59. Lun, M. P. et al. Spatially heterogeneous choroid plexus transcriptomes encode positional identity and contribute to regional CSF production. *J. Neurosci.* **35**, 4903–4916 (2015).

60. Tahira, A. et al. Are the 50's, the transition decade, in choroid plexus aging?. *Geroscience* **43**, 225–237 (2021).

61. Jensen, D. B. et al. The Na(+),K(+),2Cl(-) Cotransporter, Not Aquaporin 1, sustains cerebrospinal fluid secretion while controlling brain K(+) Homeostasis. *Adv. Sci. (Weinh.)* **12**, e2409120 (2025).

62. Boumezbeur, F. et al. Altered brain mitochondrial metabolism in healthy aging as assessed by in vivo magnetic resonance spectroscopy. *J. Cereb. Blood Flow. Metab.* **30**, 211–221 (2010).

63. Bahadur Patel, A., Veeraiah, P., Shameem, M., Mahesh Kumar, J. & Saba, K. Impaired GABAergic and glutamatergic neurometabolic activity in aged mice brain as measured by (1) H-[(13) C]-NMR spectroscopy. *FASEB J.* **35**, e21321 (2021).

64. Miccheli, A. et al. [1-13C]Glucose entry in neuronal and astrocytic intermediary metabolism of aged rats. A study of the effects of nicergoline treatment by 13C NMR spectroscopy. *Brain Res.* **966**, 116–125 (2003).

65. Silverberg, G. D., Mayo, M., Saul, T., Rubenstein, E. & McGuire, D. Alzheimer's disease, normal-pressure hydrocephalus, and senescent changes in CSF circulatory physiology: a hypothesis. *Lancet Neurol.* **2**, 506–511 (2003).

66. Jones, H. C., Deane, R. & Bucknall, R. M. Developmental changes in cerebrospinal fluid pressure and resistance to absorption in rats. *Brain Res.* **430**, 23–30 (1987).

67. Dobin, A. et al. STAR: ultrafast universal RNA-seq aligner. *Bioinformatics* **29**, 15–21 (2013).

68. Love, M. I., Huber, W. & Anders, S. Moderated estimation of fold change and dispersion for RNA-seq data with DESeq2. *Genome Biol.* **15**, 550 (2014).

69. Love, M. I., Anders, S., Kim, V. & Huber, W. RNA-Seq workflow: gene-level exploratory analysis and differential expression. *F1000Res.* **4**, 1070 (2015).

70. Robinson, M. D. & Oshlack, A. A scaling normalization method for differential expression analysis of RNA-seq data. *Genome Biol.* **11**, R25 (2010).

71. Pedregosa, F., Varoquaux, G., Gramfort, A. & & al., e. Scikit-learn: Machine learning in Python. *J. Mach. Learn. Res.* **12**, 2825–2830 - (2011).

72. Dusa, A. Package 'venn'. Vol. version 1.9 (2018).

73. Wickham, H. ggplot2. *Wiley Interdiscip. Rev. Comput. Stat.* **3**, 180–185 (2011).

74. Ashburner, M. et al. Gene ontology: tool for the unification of biology. The Gene Ontology Consortium. *Nat. Genet.* **25**, 25–29 (2000).

75. Gene Ontology Consortium et al. The Gene Ontology knowledgebase in 2023. *Genetics* **224**, iyado31 (2023).

76. Thomas, P. D. et al. PANTHER: Making genome-scale phylogenetics accessible to all. *Protein Sci.* **31**, 8–22 (2022).

77. Mi, H. et al. Protocol Update for large-scale genome and gene function analysis with the PANTHER classification system (v.14.0). *Nat. Protoc.* **14**, 703–721 (2019).

78. Cunningham, F. et al. Ensembl 2022. *Nucleic Acids Res.* **50**, D988–D995 (2022).

79. Kinsella, R. J. et al. Ensembl BioMarts: a hub for data retrieval across taxonomic space. *Database (Oxf.)* **2011**, bar030 (2011).

80. Westi, E. W., Andersen, J. V. & Aldana, B. I. Using stable isotope tracing to unravel the metabolic components of neurodegeneration: Focus on neuron-glia metabolic interactions. *Neurobiol. Dis.* **182**, 106145 (2023).

81. Andreassen, S. N., Toft-Bertelsen, T. L., Wardman, J. H., Villadsen, R. & MacAulay, N. Transcriptional profiling of transport mechanisms and regulatory pathways in rat choroid plexus. *Fluids Barriers CNS* **19**, 44 (2022).

82. Andersen, J. V., Westi, E. W., Neal, E. S., Aldana, B. I. & Borges, K. beta-Hydroxybutyrate and medium-chain fatty acids are metabolized by different cell types in mouse cerebral cortex slices. *Neurochem Res.* **48**, 54–61 (2023).

83. Westi, E. W. et al. Divergent cellular energetics, glutamate metabolism, and mitochondrial function between human and mouse cerebral cortex. *Mol. Neurobiol.* **59**, 7495–7512 (2022).

84. Kraunsoe, R. et al. Mitochondrial respiration in subcutaneous and visceral adipose tissue from patients with morbid obesity. *J. Physiol.* **588**, 2023–2032 (2010).

85. Lolansen, S. D. et al. Choroid plexus-mediated CSF secretion remains stable in aging rats via high and age-resistant metabolic activity. *Zenodo* https://doi.org/10.5281/zenodo.15687756 (2025).

Author contributions

N.M., F.D., A.P., B.A. designed the research study; S.D.L., E.O.R., S.N.A., M.T., C.S., J.H.W., M.S.P., J.V.A., E.W.W., T.L.T.B., A-.KM.L. carried out the experiments; S.D.L., E.O.R., S.N.A., M.T., J.V.A., E.W.W., A.-K.M.L. analyzed the data; S.D.L., E.O.R., S.N.A., J.V.A., N.M. drafted the manuscript, and all authors revised and approved the final version.

Competing interests

The authors declare no competing interests.

Additional information

Supplementary information The online version contains supplementary material available at https://doi.org/10.1038/s41467-025-61889-6.

Correspondence and requests for materials should be addressed to Nanna MacAulay.

Peer review information *Nature Communications* thanks Jean-François Gherise-Egea, Kristopher Kahle and the other anonymous reviewer(s) for their contribution to the peer review of this work. A peer review file is available.

Reprints and permissions information is available at http://www.nature.com/reprints

Publisher's note Springer Nature remains neutral with regard to jurisdictional claims in published maps and institutional affiliations.